Electro-Optical Platform for the Manipulation of Live Cells†

M. Ozkan,‡ T. Pisanic,§ J. Scheel,|| C. Barlow,|| S. Esener,‡ and S. N. Bhatia*,§

Department of Electrical and Computer Engineering, University of California at San Diego, La Jolla, California 92093, Department of Bioengineering, University of California at San Diego, La Jolla, California 92093, and The Salk Institute for Biological Studies, Laboratory of Genetics, La Jolla, California 92037

Received July 3, 2002. In Final Form: October 2, 2002

The advent of the genome facilitated by the advances in micro- and nanotechnology has revolutionized our understanding of living systems. DNA microarrays, catalytic RNA arrays, and protein arrays are all a consequence of innovations in engineering at the micro- and nanoscales. Here, we extend this paradigm to the fabrication of live mammalian cell arrays that can be used to investigate the state of the cell at the level of an integrated system. Specifically, we describe an electro-optical system that utilizes physical properties of mammalian cells (charge, dielectric permittivity) rather than receptor-mediated adhesion to rapidly pattern and manipulate cells in a microarray format. The platform we describe is an electro-optical method that employs two complementary methods of cell manipulation: (1) electrophoretic arraying of cells in a dc field due to their intrinsic negative surface charge and (2) remote optical manipulation of individual cells by vertical-cavity surface emitting laser driven infrared optical tweezers. The platform is optically transparent and thus enables monitoring of fluorescent reporters of cellular events (e.g., expression of green fluorescent protein) and allows remote optical manipulation of arrayed cells without risk of breaching the aseptic environment. In addition to the experimental manipulation of mammalian cells, we also present a theoretical framework to establish the limitations of the platform we describe. The ability to probe dynamic cellular events in parallel may offer insights into unforeseen biological mechanisms of cellular function and find applications in drug discovery, functional genomics, and tissue engineering.

Introduction

Live cellular arrays hold promise as platforms for pharmaceutical drug development and as fundamental tools to study cell fate and function.[1,2] To make progress toward high-throughput cell-based assays, it may be beneficial to leverage existing MEMS (microelectromechanical systems) technologies as has been done in other chip-based biosystems such as DNA microarrays,[3−5] catalytic RNA arrays,[6] and protein arrays.[7−10] Such novel, hybrid cell-based platforms should meet several design criteria: innocuous manipulation of live cells, phenotypic stability of differentiated cells, and remote detection of biological events. We and others have reported on ways to stabilize the phenotype of mammalian cells and detect cellular events;[1,11−13] however, in this study we focus on the manipulation of live cells.

Biophysical "handles" to manipulate cells can be classified as passive or active. Passive handles include surface topology and chemistry. The simplest example of surface topology to array cells is the use of physical confinement in multiwell plates. Ninety-six- and 384-well plates are available to interface with standardized detection systems; however, this technique can require large volumes of reagents and often utilizes sophisticated robotics. In addition to robotics, fluorescence-activated cell cytometry can be used to deliver cells to each well, although this can expose cells to potentially hostile handling forces. Multiwell systems allow distinct fluidic environments to exist in each well; however, this is not always required or even desired. In contrast, surface chemistry can be utilized to form planar cellular arrays, where all cells are exposed to the same fluidic environment. Surface chemistry combined with microfabrication-based technologies such as photolithography,[11,14] microcontact printing,[15−18] mi-

* To whom correspondence should be addressed. Mailing address: Sangeeta N. Bhatia, M.D., Ph.D., Departments of Bioengineering and Medicine, UCSD-MC 0412, 9500 Gilman Drive, La Jolla CA, 92093. E-mail: sbhatia@ucsd.edu. Fax: (858) 822-4203. Phone: (858)822-3142.

† Part of the *Langmuir* special issue entitled The Biomolecular Interface.

‡ Department of Electrical and Computer Engineering, University of California at San Diego.

§ Department of Bioengineering, University of California at San Diego.

|| The Salk Institute for Biological Studies, Laboratory of Genetics.

(1) Chen, C. S.; Tien, J.; Bhadriraju, K.; Nelson, C. M.; Tan, J. *Mol. Biol. Cell* **2001**, *12*, 269a.

(2) Kapur, R.; Giuliano, K. A.; Campana, M.; Adams, T.; Olson, K.; Jung, D.; Mrksich, M.; Vasudevan, C.; Taylor, D. L. *Biomed. Microdevices* **1999**, *2*, 99−109.

(3) Heller, M. J. *IEEE Eng. Med. Biol. Mag. (USA)* **1996**, *15*, 100−104.

(4) Pease, A. C.; Solas, D.; Sullivan, E. J.; Cronin, M. T.; Holmes, C. P.; Fodor, S. P. A. *Proc. Natl. Acad. Sci. U.S.A.* **1994**, *91*, 5022−5026.

(5) Ziauddin, J.; Sabatini, D. M. *Nature* (*London*) **2001**, *411*, 107−110.

(6) Seetharaman, S.; Zivarts, M.; Sudarsan, N.; Breaker, R. R. *Nat. Biotechnol.* **2001**, *19*, 336−341.

(7) MacBeath, G.; Schreiber, S. L. *Science* (*Washington, D.C.*) **2000**, *289*, 1760−1763.

(8) Yousaf, M. N.; Houseman, B. T.; Mrksich, M. *Proc. Natl. Acad. Sci. U.S.A.* **2001**, *98*, 5992−5996.

(9) Hodneland, C. D.; Lee, Y.-s.; Min, D.-H.; Mrksich, M. *Proc. Natl. Acad. Sci. U.S.A.* **2002**, *99*, 5048−5052.

(10) Lee, K.-B.; Park, S.-J.; Mirkin, C. A.; Smith, J. C.; Mrksich, M. *Science* (*Washington, D.C.*) **2002**, *295*, 1702−1705.

(11) Bhatia, S. N.; C., C. S. *Biomed. Microdevices* **1999**, *2*, 131−144.

(12) Bhatia, S. N.; Balis, U. J.; Yarmush, M. L.; Toner, M. *FASEB J.* **1999**, *13*, 1883−1900.

(13) Zlokarnik, G.; Negulescu, P. A.; Knapp, T. E.; Mere, L.; Burres, N.; Feng, L.; Whitney, M.; Roemer, K.; Tsien, R. Y. *Science* (*Washington, D.C.*) **1998**, *279*, 84−88.

(14) Bhatia, S. N.; Yarmush, M. L.; Toner, M. In *Methods in Molecular medicine*: *Tissue engineering methods and protocols*; Morgan, J. R., Yarmush, M. L., Eds.; Humana Press: Totowa, NJ, 1998; pp 349−363.

(15) Kumar, A.; Whitesides, G. M. *Appl. Phys. Lett.* **1993**, *63*, 2002−2004.

10.1021/la0261848 CCC: $25.00
Published on Web 12/02/2002

crofluidic delivery,[19−21] and stencil[22,23] patterning has been reported for fabricating such planar cellular arrays. In general, these techniques utilize chemical patterns for cell adhesion (e.g., cell adhesion proteins) and/or adhesion repellants (e.g., poly(ethyleneoxide)) on the substrate of choice.[16,24] These tools have proven to be robust and versatile; however, cell adhesion is a time-dependent process that can require hours to create an array and such techniques typically result in relatively poor "capture" efficiency (i.e., patterned cells as a fraction of cells plated). To improve capture efficiency and reduce patterning times, active methods to manipulate cells may offer some advantages.

"Active" methods for cell manipulation use some form of energy to move cells as physical objects, such as those that are polarizable or bend light. For example, dielectrophoretic patterning[25−29] has been used to rapidly (ca. seconds to minutes) manipulate or sort cells. This technique is based on the relative polarization between a cell and the surrounding medium in a nonuniform electric field. Dielectrophoresis may be useful as a tool for cell sorting and cell arraying; however, to achieve arbitrary single cell manipulation, it can require sophisticated electrode design due to the complex dependence of dielectrophoretic force on the electric field. For manipulation of single cells, optical "tweezers" that use radiation pressure of a focused laser beam to trap spherical particles have also been utilized.[30−35] While optical forces have proven to be a powerful tool for single cell manipulation, traditional optical tweezer setups require large benchtop infrared lasers and are not amenable to integration with a small, portable chip-based unit.

In this study, we describe an electro-optical method that uses two active methods of cell manipulation: (1) the intrinsic negative surface charge of mammalian cells is used to array cells by electrophoresis in an applied dc electric field and (2) vertical-cavity surface emitting lasers (VCSELs) are utilized as a miniaturized source of infrared light for optical tweezers to enable remote manipulation of arrayed cells. Specifically, we present the design and fabrication of an electrophoretic chamber that is optically transparent and therefore allows for both the integration of infrared optical tweezers and visualization of the electrophoretic arraying process (Figure 1). We first demonstrate the ability to reversibly manipulate polystyrene beads in deionized water as a "best case" condition and then apply this system to the electrophoretic arraying of live neural stem cells in physiological buffers. In addition, we employ finite element modeling, colloidal particle theory, and measurements of cell surface charge to add insight into the particle motion and distribution that we experimentally observed. Finally, we demonstrate that a VCSEL-derived optical tweezer can be utilized to remotely manipulate individual cells of interest within the array. This platform for cellular manipulation may find applications in target validation within drug development, functional genomics, and tissue engineering.

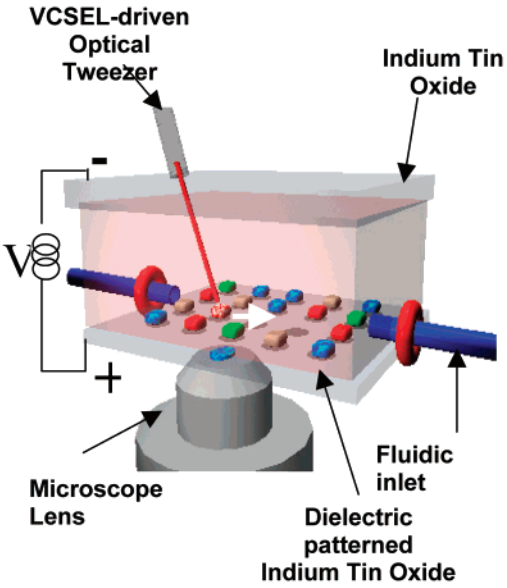

Figure 1. Schematic of electro-optical setup with hypothetical integrated fluidics. Cells are electrokinetically arrayed by application of an electric field across the top (uniform) and bottom (patterned) electrode. The bottom electrode is fabricated as seen in Figure 2. Optically transparent patterned anodes and a uniform cathode are utilized (indium−tin oxide) to facilitate microscopic visualization and allow manipulation of cells by off-chip optical tweezers driven by miniature vertical-cavity surface emitting infrared lasers.

Experimental Methods

Fabrication of Electrode Array. For experiments with polystyrene beads (Bangs Laboratories), standard photolithographic techniques were used to pattern a Si_3N_4 or SiO_2 dielectric layer on anodic silicon. In the case of electrophoretic cellular transport, agarose was used as a relative dielectric by patterning on a transparent indium−tin oxide (ITO) electrode. The process is schematically depicted in Figure 2. Briefly, a 2.5% aqueous agarose solution (NuSieve 3:1 agarose) was heated to 180 °C and syringe-filtered (Millex, 0.45 μm) before being spun onto an ITO (Delta Technologies) substrate at 2500 rpm (Headway Research photoresist spinner). Agarose was allowed to dry overnight at room temperature before spinning on a layer of photoresist (Headway Research photoresist spinner, AZ4400 positive resist, 4000 rpm), which was subsequently baked at 90 °C for 2 h. Following development (AZ 400K developer 1:3 in deionized water, 30 s), the specimens were plasma etched with oxygen (Technic 500 II Asher, 100 W) for 60−120 min, until the agarose layer was completely removed from the electrode surfaces, after which the remaining resist was removed with acetone.

Assembly and Use of the Electro-Optical Chamber. The experimental setup (Figure 1) consists of a patterned bottom

(16) Chen, C. S.; Mrksich, M.; Huang, S.; Whitesides, G. M.; Ingber, D. E. *Science* (*Washington, D.C.*) **1997**, *276*, 1425−1428.
(17) Xia, Y. N.; Whitesides, G. M. *Annu. Rev. Mater. Sci.* **1998**, *28*, 153−184.
(18) Jackman, R. J.; Wilbur, J. L.; Whitesides, G. M. *Science* (*Washington, D.C.*) **1995**, *269*, 664−666.
(19) Kim, E.; Xia, Y. N.; Whitesides, G. M. *J. Am. Chem. Soc.* **1996**, *118*, 5722−5731.
(20) Folch, A.; Ayon, A.; Hurtado, O.; Schmidt, M. A.; Toner, M. *J. Biomech. Eng.* **1999**, *121*, 28−34.
(21) Delamarche, E.; Bernard, A.; Schmid, H.; Michel, B.; Biebuyck, H. *Science* (*Washington, D.C.*) **1997**, *276*, 779−781.
(22) Folch, A.; Jo, B. H.; Hurtado, O.; Beebe, D. J.; Toner, M. *J. Biomed. Mater. Res.* **2000**, *52*, 346−353.
(23) Kane, R. S.; Takayama, S.; Ostuni, E.; Ingber, D. E.; Whitesides, G. M. *Biomaterials* **1999**, *20*, 2363−2376.
(24) Liu, V. A.; Jastromb, W. E.; Bhatia, S. N. *J. Biomed. Mater. Res.* **2002**, *60*, 126−134.
(25) Fuhr, G.; Glasser, H.; Mueller, T.; Schnelle, T. *Biochim. Biophys. Acta* **1994**, *1201*, 353−360.
(26) Mahaworasilpa, T. L.; Coster, H. G. L.; George, E. P. *Biochim. Biophys. Acta* **1994**, *1193*, 118−126.
(27) Pethig, R. *Crit. Rev. Biotechnol.* **1996**, *16*, 331−348.
(28) Matsue, T.; Matsumoto, N.; Uchida, I. *Electrochim. Acta* **1997**, *42*, 3251−3256.
(29) Voldman, J.; Braff, R. A.; Toner, M.; Gray, M. L.; Schmidt, M. A. *Biophys. J.* **2001**, *80*, 531−541.
(30) Ashkin, A. *Phys. Rev. Lett.* **1970**, *24*, 156−159.
(31) Ashkin, A.; Dziedzic, J. M. *Appl. Phys. Lett.* **1971**, *19*, 283−285.
(32) Ashkin, A. *Science* (*Washington, D.C.*) **1980**, *210*, 1081−1088.
(33) Ashkin, A.; Dziedzic, J. M.; Yamane, T. *Nature* (*London*) **1987**, *330*, 769−771.
(34) Ashkin, A.; Dziedzic, J. M. *Science* (*Washington, D.C.*) **1987**, *235*, 1517−1520.
(35) Guck, J.; Ananthakrishnan, R.; Mahmood, H.; Moon, T. J.; Cunningham, C. C.; Hallworth, R.; Kas, J. *Biophys. J.* **2001**, *80*, 277a.

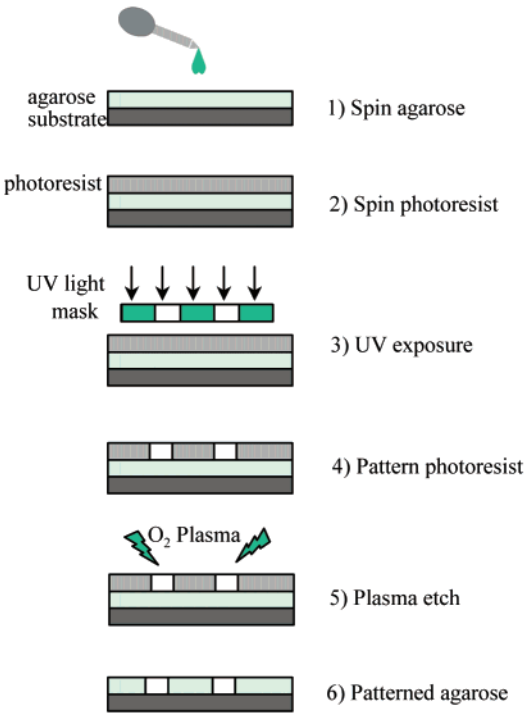

Figure 2. Agarose patterning procedure on a semiconductor substrate: (1) spin agarose, (2) spin photoresist, (3) photopattern resist, (4) develop exposed photoresist, (5) plasma etch, (6) patterned agarose film on semiconductor substrate.

electrode (anode) and an unpatterned transparent top electrode (cathode). A flat, 1 mm thick piece of silicon or poly(dimethylsiloxane) (PDMS) with an excised hole is used to create a fluid chamber between the anode and cathode. A fluid containing the objects to be arrayed can be injected into the chamber via pipet or fluidic inlets. Once sealed, a voltage is applied between the anodic and cathodic plates. Within this system, chemical energy is converted into electrical energy through redox reactions at the electrodes, resulting in the transport of ions between the electrodes and the completion of an electrical circuit. In solutions that are of approximately neutral pH, such as those we use in our electrochemical circuit, oxidation of water at the anode produces oxygen (O_2) and aqueous hydrogen ions, whereas the reduction of aqueous hydrogen ions at the cathode generates molecular hydrogen.[36] Polystyrene beads were suspended at a typical concentration of 10^6/mL. Twenty microliters of solution was applied to the chamber, and an applied voltage of 2−3 V was utilized. For experiments with mammalian cells, $(1-5) \times 10^5$ cells/mL were prepared in Krebs Ringers buffer with the following composition: 7.14 g of NaCl, 0.42 g of KCl, 0.85 g of D-glucose, 2.1 g of $NaHCO_3$, and 4.75 g of HEPES per 2 L of deionized (DI) water with a conductivity of approximately 10 mS/cm.

VCSEL-Driven Optical Tweezers Setup. A 4 × 4, 850 nm VCSEL array was obtained from Honeywell, Inc. VCSEL-derived infrared beams were collimated and focused on the sample plane by using a high-magnification microscope objective (100× magnification, 1.25 numerical aperture). A dichroic beam splitter under the microscope objective provided in situ observation of the tweezers through a CCD camera. Between the microscope objective and the chamber, a drop of index matching oil (n = 1.51) was used. VCSELs were driven with an applied current of 14 mA corresponding to approximately 3.5 mW. Cells were typically transported at a rate of 2 μm/s corresponding to an approximate trapping force of 0.1 pN.

Experimental Modeling. Quickfield (version 4.2, Tera Analysis Co.) was used to produce two-dimensional models of the electric field distribution. Quickfield solves Poisson's equations for electrostatics and current flow. Neumann boundary conditions were used for the edges of the electrodes by assuming constant voltage. Electrodes were 20 μm diameter circles. A 2 × 2 μm grid setting with 200 mesh nodes was used for the analysis. Modeling parameters were as follows: applied potential, 3 V; resistivity (ρ) of DI water, 18 MΩ cm; ρ of ITO, 10^{-4} Ω cm; ρ of Si, 10 Ω cm; ρ of SiO_2, 10^6 Ω cm.

Cell Isolation. Neural stem cells were isolated from the lateral ventrical/forebrain of an adult mouse as described previously.[37] Briefly, anesthetized mice were decapitated. Their brains were removed and placed into cold PBS. Dissections of the hippocampus and lateral ventrical/forebrain were conducted under a microscope and triturated with a medium bore (1.5−1.0 mm) pasteur pipet. Tissue pieces were further digested by a papain−protease−DNase digestion for 15 min to produce a single cell suspension. Cells were washed in PBS and were grown in DMEM:F12 with N-2 supplement, containing 20 ng/mL of both FGF-2 and EGF. Hepatocytes were isolated from 2−3 month old adult female Lewis rats (Charles River Laboratories, Wilmington, MA) weighing 180−200 g, by a modified procedure of Seglen.[38] Detailed procedures for isolation and purification of hepatocytes were previously described by Dunn et al.[39] Briefly, 200−300 million cells were isolated with viability between 85% and 95%, as judged by trypan blue exclusion. Nonparenchymal cells, as judged by their size (<10 μm in diameter) and morphology (nonpolygonal or stellate), were less than 1%. The culture medium was Dulbecco's modified Eagle's medium (DMEM, Gibco) supplemented with 10% fetal bovine serum (FBS; Sigma, St. Louis, MO), 0.5 U/mL insulin, 7 ng/mL glucagon, 20 ng/mL epidermal growth factor, 7.5 μg/mL hydrocortisone, 200 U/mL penicillin, and 200 μg/mL streptomycin.

Measurement of Cellular Zeta Potential. The potential at the shear plane around a moving spherical object in a electrolyte can be described by a quantity known as the zeta potential. It is primarily the zeta potential that determines particle velocity in electrokinetic transport phenomenon.[40] Zeta potential measurements were performed using a Pen Kem model 500 Laser Zee potential meter that measures the zeta potential of particles by visualization of particle trajectories as they move in a known electric field. The zeta potentials of various cell types were measured in KRB and then adjusted for the viscosity and dielectric properties of KRB as distinct from deionized water. The zeta potential of 20 μm diameter polystyrene beads in DI water was determined to be −80 mV. Each sample was measured approximately 10 times, and several samples for each batch were measured.

Results and Discussion

Electrophoretic Manipulation of Polystyrene Beads and Live Mammalian Cells. As a first step toward manipulating live mammalian cells, we conducted our experiments using polystyrene beads of 20 μm diameter as "model cells." Using our experimental setup, we could readily array negatively charged beads suspended in deionized water onto arbitrarily defined electrode (100 μm in diameter) patterns within 1 min of application of a 1 V bias (Figure 3A). If the electrode size was reduced to 20 μm, single bead arrays could also be produced (Figure 3B). The arraying could be reversed by reversing the applied potential (data not shown).

Following our studies with polystyrene beads, we sought to apply our arraying capabilities to living mammalian cells. Much like the polystyrene beads, mammalian cells exhibit a net negative surface charge due to charged carbohydrates and sialic acid residues in the glycocalyx.[41] Unlike inanimate beads, however, mammalian cells

(36) Sato, N. *Electrochemistry at metal and semiconductor electrodes*; Elsevier: New York, 1998.

(37) Allen, D. M.; van Praag, H.; Ray, J.; Weaver, Z.; Winrow, C. J.; Carter, T. A.; Braquet, R.; Harrington, E.; Ried, T.; Brown, K. D.; Gage, F. H.; Barlow, C. *Genes Dev.* **2001**, *15*, 554−566.

(38) Seglen, P. O. *Methods Cell. Biol.* **1976**, *13*, 29−83.

(39) Dunn, J. C.; Tompkins, R. G.; Yarmush, M. L. *Biotechnol. Prog.* **1991**, *7*, 237−245.

(40) Hiemenz, P. C.; Rajagopalan, R. *Principles of Colloid and Surface Chemistry*, 3rd ed.; Marcel Dekker: New York, 1997.

(41) Van Damme, M.-P. I.; Tiglias, J.; Nemat, N.; Preston, B. N. *Anal. Biochem.* **1994**, *33*, 62−70.

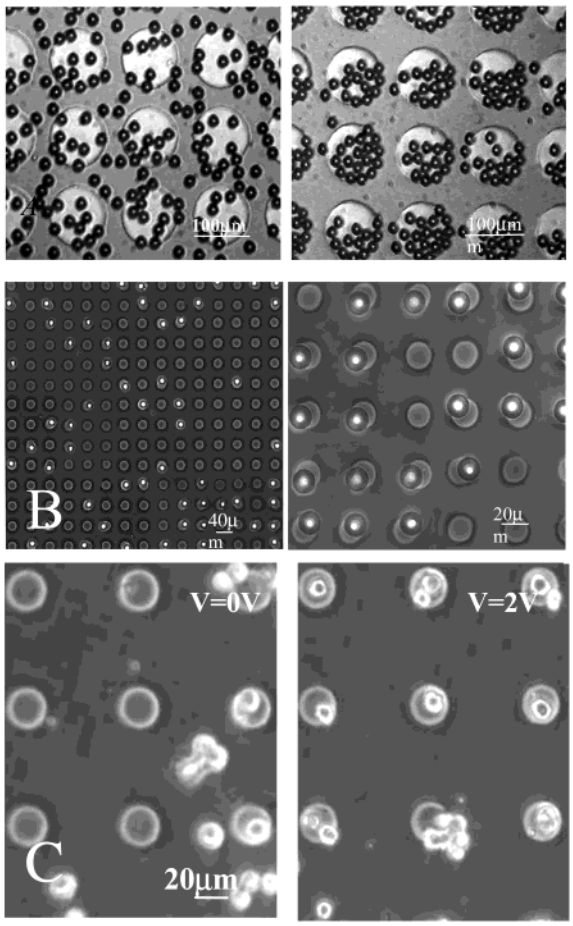

Figure 3. Electrophoretic assembly of polystyrene beads and neural stem cells. (A) Assembly of 20 μm polystyrene beads in deionized water on a silicon/silicon nitride electrode array before and after 30 s of an applied bias of 1 V. (B) Single 20 μm bead assembly in deionized water on a 25 μm diameter agarose-patterned, transparent ITO electrode array. Two magnifications of phase contrast micrographs are shown. (C) Live neural progenitor cells assembled on a 25 μm diameter agarose-patterned, ITO electrode array before and after an applied bias of 2 V for 10 min.

require osmotic equilibrium across the plasma membrane, along with other special conditions, such as a physiological pH and nutrient availability, to maintain viability. Therefore, we utilized a physiological buffer of relatively low conductivity relative to other iso-osmotic buffers (Krebs Ringers buffer, 10 mS/m) to minimize the reduction in electrophoretic transport. Initial experiments with human fibrosarcoma cells and primary rat hepatocytes demonstrated a propensity for nonspecific cell adhesion to the dielectric region of the substrate, which limited the efficiency of the assembly process. To prevent nonspecific binding, agarose (~1 μm coating of a nonadhesive hydrogel) was patterned onto the nonelectrode regions and in some experiments was used as the insulating dielectric layer itself.

Once the suspending medium was optimized and the nonadhesive layer was appropriately patterned, we used our system for a number of different cell types and applications. With an eye toward functional genomic applications in the future, we utilized our system to produce single cell arrays of murine neural progenitor cells (Figure 3C). The fragility of neural progenitor cells limits their compatibility with relatively hostile cell sorting procedures, such as fluorescence-activated cell sorting (FACS), and so provides an ideal example of the potential advantages of electrophoretic arraying. Initially, the neural progenitor cells exhibited a random distribution (Figure 3C, left). Following an applied bias of 2 V for 10 min, the progenitor cells assembled into an organized array (Figure 3C, right).

Biocompatibility of ITO. To ensure that long-term studies could indeed be accomplished on an ITO substrate, we investigated and affirmed the biocompatibility of ITO with neural stem cells. Progenitor cell growth and division were followed for 10 days after seeding on an ITO substrate. Cell growth, viability, morphology, and division were indistinguishable from those of cells cultured on polystyrene dishes for up to 10 days (data not shown).

Biocompatibility of dc Electric Fields. We initially verified the biocompatibility of small dc electric fields with cell viability by examining the effect of various field strengths on fibroblast morphology and mitotic index. Cellular response was assessed by replating 3T3 fibroblasts after exposure to a 0−20 V (0−200 V/cm) electric field for 1 min. Cells were examined under phase contrast microscopy and compared with unexposed cells for normal morphology and proliferation rate. At low voltages (1−4 V), no morphologic changes were observed (e.g., cell lysis, blebbing). Between 5 and 10 V of applied bias, filopodia-like extensions were observed. Such electric-field-induced filopodial formation has been previously reported in neurons and macrophages at similar electric field intensities.[42] At an applied bias of 20 V, the cells lysed, presumably due to destabilization of the plasma membrane (data not shown).

The platform described here bears some similarity to other platforms described in the literature.[3,43] The Nanogen system also utilizes an electronic addressing platform to manipulate DNA and living cells. In the current incarnation, the device is a planar array of individually addressable electrodes overcoated with a thin hydrogel rather than an enclosed chamber with a top counter electrode as we describe. While the Nanogen system offers the advantage of individual electrode addressability, the bottom electrode is opaque and therefore requires reflective microscopy or laser scanning for visualization. Furthermore, while the device runs in dc mode (as ours does) for the manipulation of DNA species, published reports of cellular manipulation in this platform have been limited to dielectrophoretic (ac) manipulation.[44] Aksay and co-workers[43] have also recently reported on the use of electrokinetic forces to manipulate 2 μm colloidal particles. Their platform utilizes an unpatterned, transparent ITO substrate in combination with regional photoillumination through a mask to induce regional current flow. Colloidal particles in solution were found to aggregate in crystalline arrays in the plane of the ITO electrode. This system was operated in nonconductive solution that is appropriate for inanimate particles; however, the platform presented in our study utilizes physiological buffers to preserve cellular osmotic equilibrium and does not require photoillumination to induce particle movement.

In summary, the electrophoretic platform described here facilitates rapid (ca. minutes) arraying of both polystyrene beads and living mammalian cells without obvious negative sequelae over the range of conditions that were tested. This tool may therefore provide a relatively rapid tool for

(42) Williams, C. V.; Davenport, R. W.; Dou, P.; Kater, S. B. *J. Neurobiol.* **1995**, *27*, 127−140.
(43) Hayward, R. C.; Saville, D. A.; Aksay, I. A. *Nature* (*London*) **2000**, *404*, 56−59.
(44) Huang, Y.; Ewalt, K. L.; Tirado, M.; Haigis, T. R.; Forster, A.; Ackley, D.; Heller, M. J.; O'Connell, J. P.; Krihak, M. *Anal. Chem.* **2001**, *73*, 1549−1559.

arraying cells to facilitate parallel monitoring for cell-based assays. The process is reversible over short time frames (ca. minutes) and does not require the use of specific cell adhesion molecules. Furthermore, the transparent platform enables observation of dynamic changes in fluorescence on standard microscopic platforms and could therefore be applied to real-time assays of gene expression using fluorescent reporters (e.g., green fluorescent protein). The ability to monitor multiple cells in parallel, and in aseptic conditions, could enable the simultaneous monitoring of populations of cells (e.g., a retroviral library) to various stimuli such as drug candidates, hormones, toxins, or differentiation cues.[13] During our platform development, we made several observations that we wish to further explore: cells appear to localize on the electrode−dielectric interface, different cellular species moved at different speeds under the same applied potential, and cells moved in both lateral and vertical directions despite the application of only a vertical electric field. To explore these phenomena, we established a theoretical framework to describe cell movement in our system.

Finite Element and Theoretical Model of the Electric Field. To gain insight into the particle motion and final distribution that we experimentally observed, we employed finite element modeling of the electric field distribution within the chamber, colloidal particle theory to predict particle velocity in the resulting field, and experimental measurements of the zeta potential of cells in buffer solutions.

The velocity of a charged particle in solution under the influence of an applied electric field can be described by the following relationship derived from colloid theory:

$$v_{\mathrm{E}} = \frac{E}{4\pi}\int_0^{\psi}\frac{\epsilon}{\eta}\,\mathrm{d}\psi$$

where E is the vector electric field strength, ϵ is the dielectric constant of the solution, η is the fluid viscosity, and ψ is the double-layer potential of the particle in solution.[45] Under certain conditions, this can be simplified in the following form:

$$v_{\mathrm{EP}} = F(\kappa^{-1}a)\frac{\epsilon\zeta}{\eta}E$$

where v_{EP} is the electrophoretic velocity that depends on the E field, F is a constant (dependent upon the Debye length (κ^{-1}) and particle radius (a)), and ξ is the zeta potential. These equations describe a steady-state condition where electrophoretic forces are counterbalanced by fluidic drag, gravity is neglected, objects are spherical, and the double-layer potential is equivalent to the zeta potential (ζ) of the particles in solution.

To predict particle velocity in our chamber, we first simulated the electric field distribution. Here we present the effect of a 20 μm electrode array on the electric field distribution inside the chamber under an applied potential of 3 V. A vertical cross section of the electric field distribution reveals that the field is maximal at the dielectric−electrode interface in both vertical and lateral directions (Figure 4A−C). A particle that is directly above either the dielectric or the electrode should migrate, under the influence of a vertical and lateral electric field, toward the electrode−dielectric interface. This is in agreement with our experimental results that demonstrate a propensity for our system to produce patterns of objects aligned near the edges of the electrode surfaces.

(45) Sennett, P.; Olivier, J. P. *Ind. Eng. Chem.* **1965**, *57* (8), 32−50.

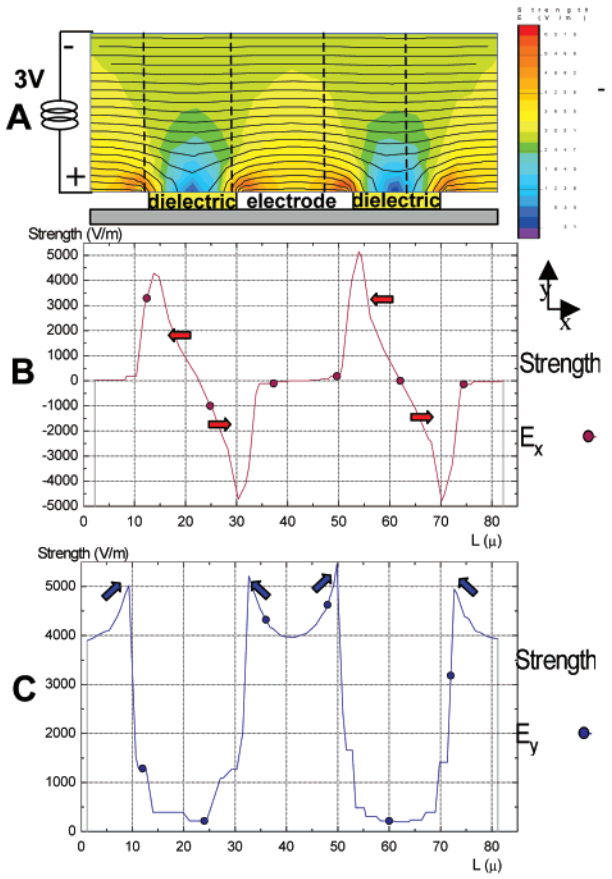

Figure 4. (A) Cross-sectional 2-D finite element model of a silicon nitride patterned silicon/deionized water/ITO system at an applied bias of 3 V; the electrode and dielectric size is 20 μm. (B) Lateral electrode field profile across the anodic surface. (C) Vertical electric field profile across the anodic surface. Arrows indicate the direction of electrokinetic force in (B) and (C). This model predicts the electrokinetic behavior of objects within the system shown in Figure 3.

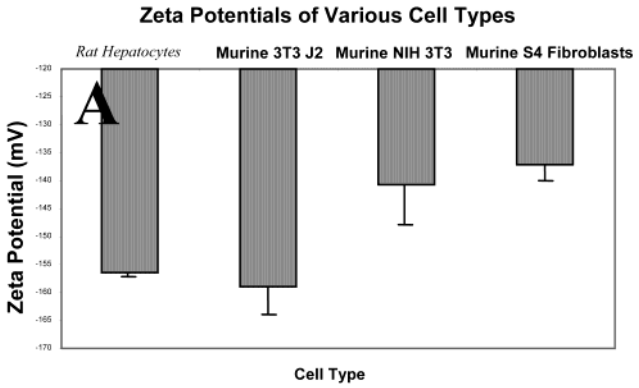

Figure 5. Zeta potentials of various cell types in KRB, measured with a Laser Zee zeta potential meter. Error bars represent standard deviation.

To map the role of electric field distribution to cell velocity, we measured the zeta potential of mammalian cells in physiological buffers (Figure 5). Note that all zeta potentials are negative, correlating with a net negative surface charge, presumably due to the glycocalyx. The most highly negative cells were primary rat hepatocytes with a zeta potential of approximately −156.4 mV as compared to murine fibroblasts such as S4 with a zeta potential of −136.9 mV. Using our model predictions, under an applied potential of 3 V in KRB, in the absence of gravitational effects and assuming similar cell diam-

eters, S4 cells would move at a steady-state velocity of approximately 0.19 μm/s as compared to a hepatocyte velocity of approximately 0.22 μm/s. This difference in velocity corresponds to 105 s for S4 cells to travel from the dielectric to the electrode ($\sim$20 μm) as compared to 90 s for hepatocytes under similar conditions. These results were qualitatively confirmed with hepatocytes patterning more rapidly than S4 cells.

While we have focused primarily on electrophoretic forces in our system, other physical forces may play a significant role. In particular, electroosmotic forces that cause fluid movement relative to a surface can occur due to the mobility of ions in solution. Electroosmotic forces are commonly utilized in capillary electrophoretic separation, where the capillary wall contains fixed charges that attract mobile ions in the fluid phase. The movement of mobile ions under an applied potential is manifested as bulk fluid motion that acts to entrain particles to be separated.[46] Thus, in the chamber presented here, the patterned anode can induce electroosmotic flow and particle entrainment in the plane of the electrode thereby contributing to the formation of a particle pattern that is congruent with the electrode pattern.

To compare the relative role of electrophoretic and electroosmotic forces in the motion of particles in our system, we compared the maximum theoretical electrophoretic velocity (which occurs in the vertical direction) to the maximum theoretical electroosmotic velocity (which occurs in the plane of the patterned anode) in the lateral direction. Our results indicate that a 20 μm polystyrene bead would move maximally at 1.6 μm/s due to electrophoretic forces alone and 0.3 μm/s due to electroosmotic forces alone. These predictions neglect gravity and were performed for 20 μm diameter polystyrene beads with a zeta potential of -80 mV in DI water using a 20 μm diameter circular electrode array with an applied bias of 3 V. Our results therefore indicate that in the absence of gravity, electrophoresis is responsible for the majority of the movement of the suspended particles through the solution though electroosmosis may play a role in the plane of the bottom electrode. A similar balance of forces between electrophoretic and electroosmotic phenomena may play a role in the electrokinetic assembly of colloidal crystals into "crystalline" colloidal arrays mentioned previously.[43]

To compare the motion of different cell types and the final distribution of patterned cells, we have focused on the effects of electrokinetic phenomena: electrophoresis and electroosmosis. We combined finite element modeling of the electric field, measurements of cellular zeta potential, and colloid theory in a comparative analysis of bead and cell movement in our system. These simulations made it possible to study the effects of the solution properties, 2-D electrode configuration, and cell properties such as concentration, charge, and size (data not shown). Nonetheless, mammalian cells are of 10$-$20 μm in diameter and thus are significantly larger than colloidal particles. As a result, gravitational forces play a significant role in the sedimentation of cells to the bottom plane. Currently, we are incorporating gravitational effects during electronic arraying of cells into our model.

VCSEL-Driven Optical Tweezers for Manipulation of Cells. To demonstrate the feasibility of integrating electronic arraying techniques with optical manipulation by VCSEL-driven optical tweezers, 3T3 mouse fibroblasts were utilized. Red- and green-labeled fibroblasts were prepared separately and mixed together in KRB solution to represent a prototypic heterogeneous cell population. About 40 μL of this solution was then injected into the system. The transparency of the agarose-patterned ITO anode allowed for real-time, parallel monitoring of live fluorescent cells with an inverted microscope. Cells were electrically arrayed onto a 50 $\times$ 50 μm electrode array, the field was turned off, and a single red cell was selected to be optically repositioned with the VCSEL-driven optical tweezers (Figure 6A,B). In addition to fibroblasts, we also demonstrated the optical manipulation of primary rat hepatocytes within our system (Figure 6E$-$H). The velocity of hepatocyte motion was limited to 2 μm/s before "falling" out of the optical trap.

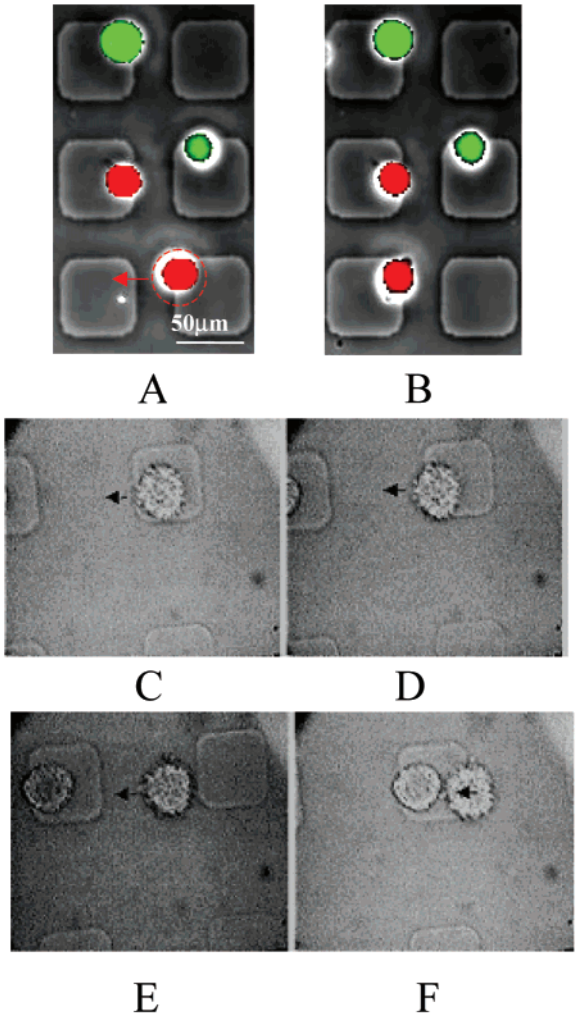

Figure 6. Optical manipulation of electrophoretically arrayed mammalian cells. (A) Dual-labeled murine fibroblasts. (B) Manipulation of a single cell (to the neighboring electrode) via VCSEL-driven optical tweezers. (C$-$F) Optical manipulation of an electrophoretically arrayed primary rat hepatocyte, showing transport of the cell by VCSEL-driven optical tweezers to the neighboring electrode. Optical manipulation of preassembled live cells enables selection of individual cells or groups of cells for capture and conventional molecular characterization.

In VCSEL-driven optical tweezers, as in conventional optical tweezers, the momentum transfer associated with the redirection of light at the object interface is transferred to the object, thus generating a physical force that can be used to trap and move the object.[30$-$35] Experimentally, the trapping force of a given laser beam can be measured

(46) Jorgenson, J. W.; Lukacs, K. D. *Science* (*Washington, D.C.*) **1983**, *222*, 266$-$272.

by the ability to "trap" an object as it moves through an aqueous solution at constant velocity. For example, we measured the ability to trap a polystyrene sphere suspended in deionized water by measuring the maximum achievable bead velocity and using Stokes' drag law: $F = 6\pi\eta r v$, where F is the drag/trapping force, η is the fluid viscocity, r is the particle radius, and v is the maximum recorded velocity. Our results indicate that the VCSELs can generate a force strong enough to move and manipulate cells up to 10 μm in diameter (approximately 0.2 pN) at a power of 3.52 mW. To minimize biological damage due to radiant energy, the VCSELs used in our experiments were operated at a near-infrared wavelength (850 nm), where a window of transparency for biological materials arises.[47]

In summary, we have experimentally and theoretically explored the ability of miniature lasers to interface with electronic arrays. Specifically, we have demonstrated that individual living cells can be selected remotely by a user and manipulated without compromising chamber sterility as may be introduced by mechanical micromanipulators. Despite their miniature size and portability, one potential limitation of VCSEL-driven optical tweezers is the relatively low output power compared to benchtop lasers. Our predictions indicate that current power limitations could limit VCSEL-driven optical tweezers to use with cells that are smaller 10 μm in size. Larger cells would require more force to overcome the increased drag force, lower velocity of transfer, or lower viscosity solution to be manipulated efficiently. Currently, we are investigating the ways of improving power output from each VCSEL or combining VCSEL beams to enable their use in manipulation of larger cells. In the future, since large arrays (32×32) of VCSELs are now commercially available, this system has the potential to be extended to the parallel manipulation of many cells simultaneously.

Conclusions

We present an electro-optical platform for the rapid parallel arraying and subsequent serial manipulation of living mammalian cells. Key features of the platform are the ability to visualize cells on standard biological microscopes (both transmitted light and fluorescence) and the capability to remotely manipulate cells of interest without compromising chamber sterility. This approach complements the existing repertoire of both passive and active techniques for cellular arraying on surfaces. In particular, the platform presented here may enable parallel interrogation of cell populations for cell-based assays in drug development and functional genomics. In the future, incorporation of electrophoretic arraying and/or VCSEL-driven optical tweezers in chip-based biosystems may further enhance the functionality of these devices.[48−51]

Acknowledgment. We thank N. LaPrath and J. Felix for their assistance with cell culture, J. Talbot for use of the zeta potential meter, and M. Wang for use of his VCSEL array setup. Support by grants from the DARPA CHIPS Center, The David and Lucile Packard Foundation (M.O., T.P, S.E., and S.B.), NIH NIDDK (S.B.), and NIH Fellowship F31 NS10860-03 (J.S. and C.B.) is acknowledged. We also thank Fred H. Gage, Jasodhara Ray, and Bobbie Miller for advice and assistance with neural progenitor cell isolation.

LA0261848

(47) Svoboda, K.; Block, S. M. *Annu. Rev. Biophys. Biomol. Struct.* **1994**, *23*, 247−285.
(48) Preckel, T.; Chan, S.; Wang, B.; Donley, A.; Bek, F.; Pfleger, M.; Hahnenberger, K. *FASEB J.* **2001**, *15*, A531.
(49) Fu, A. Y.; Spence, C.; Scherer, A.; Arnold, F. H.; Quake, S. R. *Nat. Biotechnol.* **1999**, *17*, 1109−1111.
(50) Ferguson, J. A.; Boles, T. C.; Adams, C. P.; Walt, D. R. *Nat. Biotechnol.* **1996**, *14*, 1681−1684.
(51) Sundberg, S. A. *Curr. Opin. Biotechnol.* **2000**, *11*, 47−53.